Available online at www.sciencedirect.com
ScienceDirect
Catalysis Today 133–135 (2008) 420–427
CATALYSIS TODAY
www.elsevier.com/locate/cattod

Effect of the preparation method on the catalytic activity of $La_{1-x}Ca_xFeO_3$ perovskite-type oxides

Gina Pecchi [a,*], Patricio Reyes [a], Raúl Zamora [a], Claudia Campos [a], Luis E. Cadús [b], Bibiana P. Barbero [b]

[a] *Departamento de Físico-Química, Facultad de Ciencias Químicas, Universidad de Concepción, Casilla 160-C, Concepción, Chile*
[b] *Instituto de Investigaciones en Tecnología Química (INTEQUI), UNSL-CONICET, Universidad Nacional de San Luis, Casilla 290, 5700 San Luis, Argentina*

Available online 26 December 2007

Abstract

$La_{1-x}Ca_xFeO_3$ ($x = 0.0$, 0.1, 0.2, 0.3, 0.4) perovskites prepared by two different methods, via precursor of citrate and via co-precipitation in basic medium, both calcined at 973 K have been investigated as catalysts for acetyl acetate and methane combustion. In the case of the citrate method, atomic absorption spectroscopy (AAS), BET specific area measurements, XRD analysis, Raman, SEM, FTIR, TPR and TPD of O_2 suggest that a continuous substitution of calcium by lanthanum in the perovskite structure is reached. In the basic series, the insertion of calcium in the $LaFeO_3$ lattice produces a substitution only up to $x = 0.1$. Higher calcium addition leads to segregated calcium phases. In the methane reaction, the substituted perovskites exhibit lower activity than the simple $LaFeO_3$ perovskite, without the preparation method effect and extent of substitution. Meanwhile, for the acetyl acetate reaction, the most active perovskite (i.e., the lower ignition temperature) was obtained in the higher substituted $La_{1-x}Ca_xFeO_3$. For the basic series, the activity in the acetyl acetate combustion decreases as the substitution degree increases up to $x = 0.2$. At higher calcium content, the activity does not change. Therefore, perovskite catalyst activity mainly depends on the composition, preparation method and nature of the compound to be combusted.

Keywords: Lanthanum; Iron; Calcium; Perovskites; Combustion; Acetyl acetate; Methane

1. Introduction

Metal oxides with a perovskite structure have been consistently proposed during the last two decades as alternative catalysts for the deep oxidation of hydrocarbons. The use of these materials has been especially advocated in applications involving high temperatures and oxygen steam-rich atmospheres, where their thermal stability comes into play. This was recognized since the early 1970s when perovskites were proposed as promising automobile exhaust catalysts [1] with a lower cost in comparison with their noble metal counterparts.

For this reason, metal-oxide catalysts have received wide attention, particularly, hexa-aluminate and perovskite-type compounds [2,3], which have even been incorporated into the design of novel combustors [4,5].

Perovskites can be represented by the general formula ABO_3 structures, where A is a large cation and B is a small cation of the d-transition series. The number of potentially interesting perovskites in the oxidation reactions is very great, owing to the number of A and B cations that can enter into this structure. It is well known that perovskite-like, mixed oxide substitution of the trivalent A-site metal ion with a bivalent or tetravalent metal cation (A′) is accompanied by a modification of the oxidation state of the B-site metal cation, thus modifying catalytic activity. Moreover, modification of the oxidation state of the B-site metal cation by insertion of A′ may be accompanied by the formation of structural defects, thus leading to non-stoichiometry. In the Co-containing perovskites, this usually means oxygen defects, while in Mn-perovskites it results in oxygen excess [6]. Fe-based [7] and Ni-based perovskites [8] were shown to have an intermediate behaviour. Formation of anionic

* Corresponding author.
E-mail address: gpecchi@udec.cl (G. Pecchi).

0920-5861/$ – see front matter
doi:10.1016/j.cattod.2007.11.011

vacancies seems to be easier than oxidation of Ni^{3+} to Ni^{4+} since the ionic radius of oxidised species does not fit the perovskite structure. Still, the best catalytic performances in catalytic combustion are exhibited by La- or La_xSr_{1-x}based perovskites containing Co, Fe or Mn as B cation [9,10]. The greatest limitation for their application is their low surface area, which appears to be a serious disadvantage for their application. In order to increase the specific surface area, various preparation methods for conventional $A_{1-x}A'_xBO_{3-\delta}$ perovskites have been investigated [11–14].

In this work, $La_xCa_{1-x}FeO_3$ ($x = 0.0$, 0.1, 0.2, 0.3, 0.4) perovskites prepared by precursor citrate and co-precipitation in basic medium are characterized and evaluated in catalytic combustion reaction. The effect of lanthanum substitution by calcium on the physical, chemical and catalytic properties for the total combustion of acetyl acetate and methane was studied.

2. Experimental

2.1. Preparation of the catalysts

$La_{1-x}Ca_xFeO_3$ ($x = 0.0$, 0.1, 0.2, 0.3, 0.4) perovskites were prepared via two different methods: the co-precipitation of the respective nitrates in a basic medium and the amorphous citrate precursor method. The first method consists in a co-precipitation of 0.1N aqueous solution of the corresponding nitrates with 0.1N sodium hydroxide solution as precipitant agent. The precipitation was performed at room temperature at pH 10 with 48 h of ageing time. The resulting precipitate was filtered off, washed with distilled water to remove excess sodium ions up to constant conductivity values, and dried overnight at 383 K in air. In the precursor citrate method, stoichiometric amounts of an aqueous solution of the nitrates of the corresponding metals were mixed with a 10% of excess in equivalent of an aqueous solution of citric acid. The resulting mixture was stirred for 15 min at room temperature and evaporated at 343 K until gel formation is reached. Then it was dried in an oven, slowly increasing the temperature up to 523 K and maintaining it overnight. The resulting powders, amorphous citrate precursor and basic precipitate, were crushed and sieved to obtain the required particle size (<200 μm). Finally, the solids were calcined at 973 K in air for 6 h. The samples were labelled as $La_{1-x}Ca_xFeO_3$ *y*, where *x* refers to the amount of Ca and *y* the preparation method, B: co-precipitation in basic medium and C: citrate precursor method.

2.2. Characterization

Atomic Absorption Spectroscopy (AAS) was performed using a PerkinElmer instrument model 3100 to determine the lanthanum, calcium and iron composition of the bulk. The specific surface areas were obtained from nitrogen adsorption isotherms at 77 K in an automatic Micromeritics apparatus Model ASAP 2010, and were evaluated using the BET equation. SEM micrographs were obtained in a JEOL model JSM 6380 LV. The Raman spectra were collected in a JASCO TRS600SZP multichannel monochromatic spectrometer using an Ar-ion laser (514.5 nm) operated at 50 mW. X-ray diffraction patterns were obtained on a Rigaku diffractometer using a Ni-filter and Cu $K\alpha_1$ radiation. The crystalline phases were identified by reference to the powder diffraction data (PDF files). TPR and oxygen TPD experiments were performed in a TPR/TPD 2900 Micromeritics system with a thermal conductivity detector. For the TPR experiments, the reducing gas was a mixture of 5%H_2/Ar (40 $cm^3\ min^{-1}$) and a heating rate of 10 K min^{-1} was employed. For the TPD experiments the samples were exposed to oxygen for 1 h at 973 K, following by cooling to room temperature in the same atmosphere. After switching the atmosphere to a helium flow, the sample was heated at a constant rate of 10 K min^{-1} and the oxygen desorbed was monitored with a thermal conductivity detector. FTIR spectra were recorded in a Nicolet Magna-IR 550 instrument, equipped with a quartz sample holder with KBr windows. The perovskites were dehydrated at 483 K and finely ground in an agate mortar with KBr to obtain a perovskite–KBr ratio 1/150.

2.3. Catalytic activity

The catalytic activity evaluation in the combustion of methane and acetyl acetate was performed in a conventional flow reactor at atmospheric pressure. In each experiment, 100 mg of catalysts diluted with 100 mg of silica as an inert was used. The activity was measured at different temperatures. The reactant mixture was fed into the reactor at 50 ml min^{-1} and the temperature was lineally increased up to 423 K, and then maintained constant for 30 min. Then, it was raised to a new isothermal temperature using the same heating rate (1 K min^{-1}). Several isothermal steps were performed until reaching complete conversion. The used reactant gaseous mixture was CH_4:O_2:He = 1:4:95 for methane combustion and $C_4H_8O_2$:O_2:He = 1:10:89 (molar) for acetyl acetate combustion. Reactor effluents were analysed using an on-line gas chromatograph Hewlett Packard model HP 4890D with thermal conductivity detector that works at a temperature of 423 K and a current of 150 mA. The column used was a 30-m capillary Supelco 25462. The carrier gas (He) flow through the column was 4 ml min^{-1} and the injector temperature at 423 K. A Quadrupole Mass Spectrometer Shimadzu, GCMS-QP5050 model was used to detect small traces of products.

3. Results and discussion

Table 1 summarises the chemical composition (nominal and experimental) for the samples calcined at 973 K, expressed as weight %. It can be seen that experimentally determined iron contents are in good agreement with the expected values in the series of samples prepared by the citrate method. In the basic method, there is agreement only for $x = 0.0$ and 0.1. For higher values, the experimental Fe content is lower than the nominal ones. The calcium content trends follow the expected values for both series, presenting lower values for the basic series. These results show an appropriate agreement with the nominal values, especially in the perovskites obtained from the citrate method.

Table 1
Iron, lanthanum and calcium bulk wt% (nominal in parenthesis), specific BET area and structure for $La_{1-x}Ca_xFeO_3$ perovskites

	Fe	La	Ca	S_{BET}	Structure
$LaFeO_3$-B	23.2 (23.0)	58.0 (57.2)	–	20.9	P
$La_{0.9}Ca_{0.1}FeO_3$-B	24.2 (24.0)	54.2 (53.7)	1.5 (1.7)	14.0	P
$La_{0.8}Ca_{0.2}FeO_3$-B	21.8 (25.0)	54.2 (49.8)	2.6 (3.6)	8.3	P + $CaCO_3$
$La_{0.7}Ca_{0.3}FeO_3$-B	20.6 (26.2)	47.8 (45.6)	4.2 (5.6)	5.4	P + $CaCO_3$
$La_{0.6}Ca_{0.4}FeO_3$-B	20.4 (27.5)	44.0 (41.0)	6.1 (7.9)	8.3	P + $CaCO_3$
$LaFeO_3$-C	23.0 (23.0)	58.2 (57.2)	–	19.5	P
$La_{0.9}Ca_{0.1}FeO_3$-C	23.0 (24.0)	55.9 (53.7)	1.3 (1.7)	17.8	P
$La_{0.8}Ca_{0.2}FeO_3$-C	24.0 (25.0)	51.9 (49.8)	3.3 (3.6)	38.6	P
$La_{0.7}Ca_{0.3}FeO_3$-C	25.6 (26.2)	47.1 (45.6)	5.3 (5.6)	38.6	P
$La_{0.6}Ca_{0.4}FeO_3$-C	26.4 (27.5)	43.5 (41.0)	7.4 (7.9)	31.2	P

P: perovskite structure.

Surface area values are also compiled in Table 1. For the simple $LaFeO_3$ perovskite, similar values of specific area are obtained, independent of the preparation procedure. With the citrate method, the solids obtained had higher surface area, ranging from 19 to 39 $m^2\ g^{-1}$ as the calcium content varies from 0.0 to 0.4. For the basic method, a large decrease in the surface area with the degree of substitution was observed. The great differences of these values depending on the preparation method show perovskite crystal growth's high sensitivity on preparation conditions. The SEM results confirm these differences with the micrographs showing substantial differences in perovskite morphology. Particle agglomerates were observed in the basic method series, while perfectly defined laminar-type structures were observed in the citrate method series.

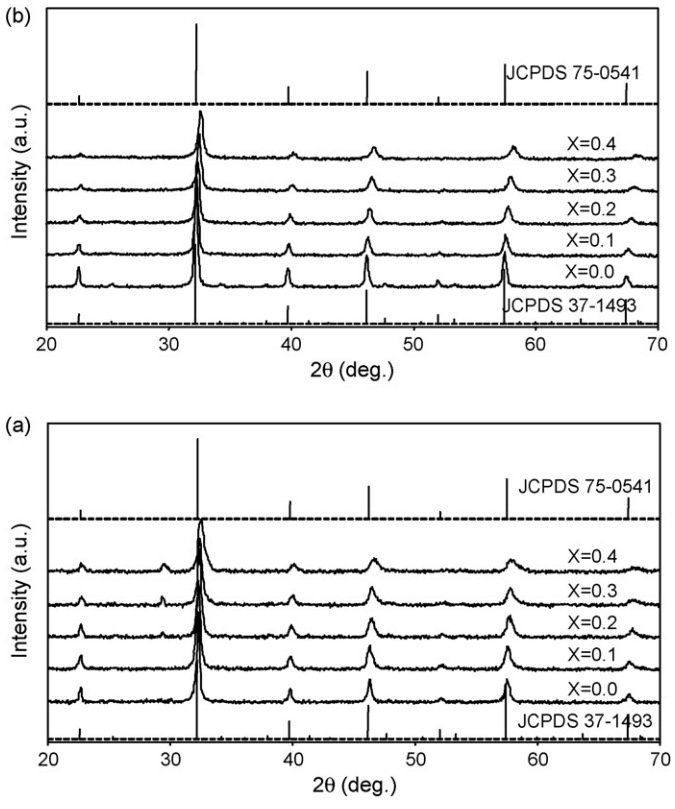

Fig. 1. X-ray diffraction patterns of $La_{1-x}Ca_xFeO_3$ perovskites: (a) basic method, (b) citrate method.

Fig. 1 summarises the XRD patterns of the prepared perovskites. Sharp reflections located at the expected 2θ values confirm that the perovskite structure was obtained after calcination of the solids at 973 K for both the citrate and basic methods. An orthorhombic $LaFeO_3$ perovskite structure is obtained, in agreement with PDF file 37-1493 with absence of extra phases. Changes depending on the calcium substitution can also be observed. Thus, as the degree of Ca substitution increases, a definite shifting towards larger 2θ angles, corresponding to lattice contraction, appears in the XRD patterns. The substitution for La^{3+} with a cation of lower oxidation state, Ca^{2+}, causes an electronic unbalance in the perovskite lattice that can be compensated by the generation of oxygen vacancies and/or the formation of Fe^{4+} ions [15–17]. The ionic radius of Fe^{4+} (0.585 Å) is smaller than that of Fe^{3+} (0.645 Å) [18] explaining the lattice contraction observed by XRD. Fig. 2(a) and (b) shows the shift of the 2θ values,

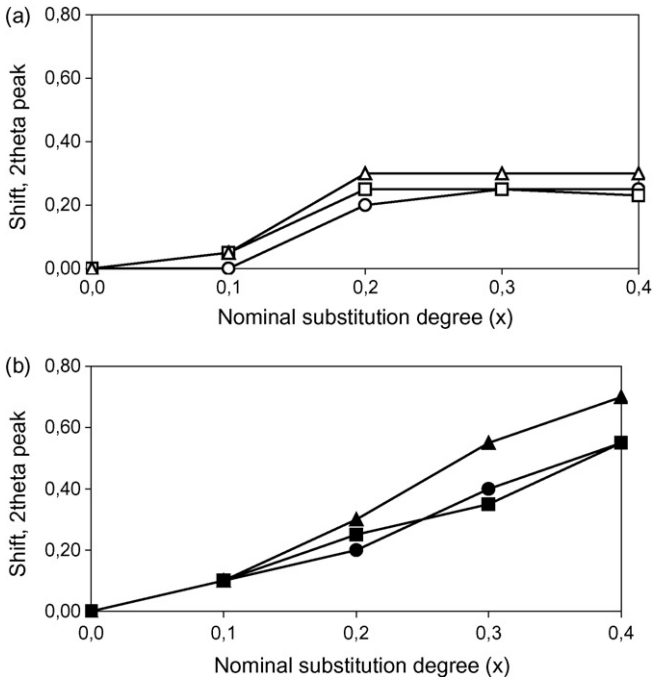

Fig. 2. Peak position shift as a function of the substitution degree: (a) basic method: 2θ (○) 40°; (□) 46 °; (△) 58°, (b) citrate method: 2θ (●) 40°; (■) 46°; (▲) 58°.

corresponding to the Bragg angles of 40°, 46° and 58°, as a function of the degree of calcium substitution for all the prepared perovskites. A linear shift with calcium substitution suggests that the insertion of calcium in the citrate method gradually increases in the studied range, whereas this increases in the basic method only occurs up to $x = 0.2$. At higher x values, a segregation of other calcium phases should occur. In the citrate method, it should also be mentioned that changes from the orthorhombic structure towards a nearly cubic one run in parallel with the increases of x values [15,17]. Furthermore, in the basic series for $x \geq 0.2$, a separate $CaCO_3$ phase can be seen, at $2\theta = 29.45°$, supporting the previous discussion that calcium is not totally incorporated into the perovskite lattice prepared with the basic medium. These results indicate that the citrate method leads to a greater extent of substitution of calcium by lanthanum, maintaining the perovskite structure with a slight distortion. Conversely, oxide segregation on the surface with lower surface area in the basic method is responsible of these lower values. Average particle size of the perovskite evaluated using the Debye Scherrer equation has displayed a decrease in the perovskite particle as the substitution with calcium increases. Thus, the diameter decreases from 6.5 to 4.0 nm in the perovskites prepared by the citrate method, whereas the observed value decreases from 6.3 to 3.0 nm as x increases in the basic method. These results are in agreement with those previously discussed for surface area and SEM.

Raman results also support the previous explanation. The Raman spectra of the $La_{1-x}Ca_xFeO_3$ perovskite prepared by the citrate method do not show band. In the perovskites prepared in the basic method, only the samples $La_{1-x}Ca_xFeO_3$, with $x \geq 0.3$, display a band at 326 cm^{-1}. Chang [19] found a similar band at 352 cm^{-1} for CaO and a band at 326 cm^{-1} attributed to mixed oxides of the type $CaHgO_2 \cdot xHgO$ and $CaHgO_2$. It should be considered that in other characterization results, this band could be attributed to the presence of a segregated phase of calcium. As discussed previously, it is proposed that the segregated $CaCO_3$ phase on the perovskite structure is present for higher x values in the basic method perovskites.

IR spectra of the prepared perovskites are presented in Fig. 3(a) and (b). The bands at 1565 and 1440 cm^{-1} are assigned, respectively, to the asymmetric and symmetric O–C–O stretching vibration of the carboxylate group [20]. In the citrate series, this band appears as a doublet rather a low intensity, broad band; whereas this band appears in the same region but with higher intensity in the basic medium series. The fact that the intensity of this band increases with the calcium content supports the hypothesis of calcium segregation in this latter series. A small band at 865 cm^{-1}, due to O–C–O bending in the carbonates, can also be observed for the substituted citrate perovskites. It appears as a shoulder for $x = 0.1$ and increases linearly when $x \geq 0.2$, but without showing any change in the wavelength. In the basic series, this band appears only when $x \geq 0.2$, with low intensity, and remains constant. Therefore, it can be assumed that this important band is related with calcium and corresponds to the out-of-plane bending of the carbonate ions. Fig. 4(a) displays this band intensity obtained from the area under the curve as a function of the substitution degree. The dependence observed has trend similar to the previously discussed XRD results regarding calcium incorporation in the perovskite structure. Similar results have been reported by Berger et al. [21] for $La_{1-x}Sr_xCoO_3$ perovskites.

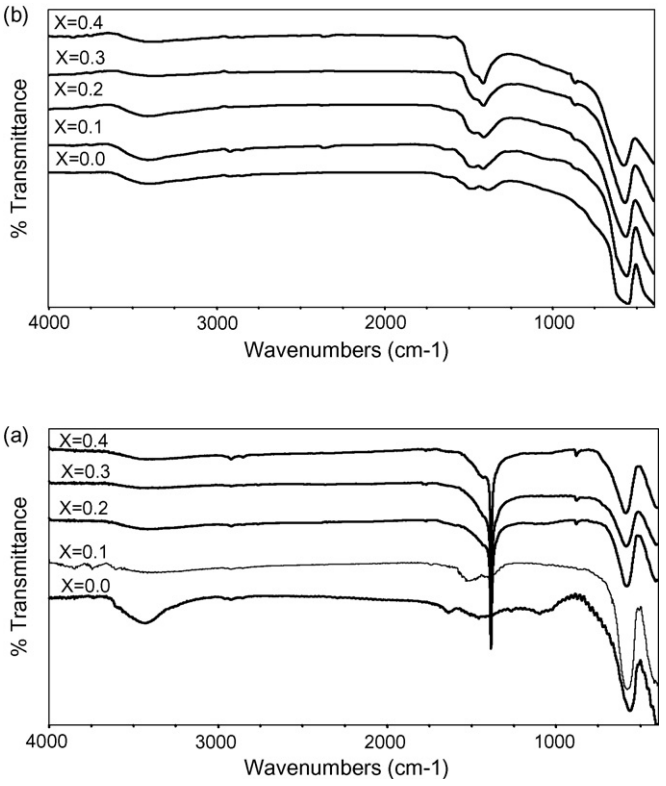

Fig. 3. IR spectra for $La_{1-x}Ca_xFeO_3$ perovskites: (a) basic method, (b) citrate method.

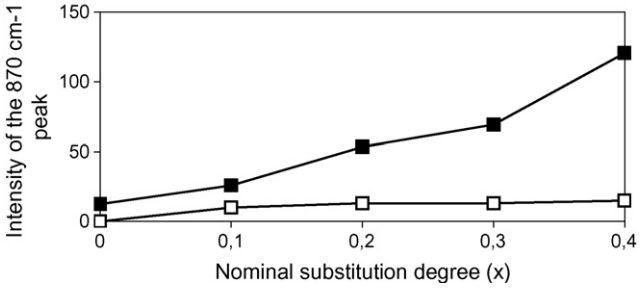

Fig. 4. Intensity of the 870 cm^{-1} peak as a function of the substitution degree: (□) basic method; (■) citrate method.

Previous reports have pointed out the importance of the evolution of oxygen during temperature-programmed desorption experiments dealing with the redox properties of these kinds of solids. Fig. 5 presents the oxygen TPD for the citrate method perovskites, where the desorption rate calculated from the oxygen concentration in the eluant gas is plotted against the catalyst temperature. For both preparation methods, the shape of the curves basically indicate a first desorption peak at temperatures lower than 373 K corresponding to the physisorbed oxygen species. Similar peaks were previously reported

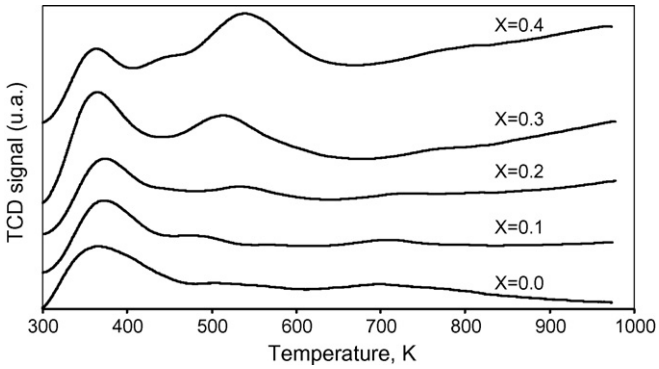

Fig. 5. Oxygen profile spectra for $La_{1-x}Ca_xFeO_3$ perovskites prepared by the citrate method.

for other substituted perovskites [22,23]. A second peak, which appears as a shoulder for the pure $LaFeO_3$ perovskites, is observed at 573 K and is attributed to the so-called α oxygen. This second peak is related to the substitution of calcium in the perovskite and increases in intensity as the substitution degree increases in the citrate series. Additionally, a slight shift towards higher temperatures was observed as x values increase. For the basic series, this peak appears only as a shoulder with virtually the same intensity for all the series. In all the TPD-substituted profiles, an important desorption of oxygen takes place at temperatures higher than 700 K for the more substituted perovskites, corresponding to the so-called β oxygen, which is associated with the lattice oxygen, Zhao et al. [24], or with oxygen species occupying the inner vacancies created by substitution of calcium by lanthanum. Therefore, this oxygen can be related to the redox properties of the perovskite. TPD–MS experiments confirm that the evolved gas and the He flow only contain oxygen. In the basic series, it appears only for the substituted perovskites with large values of x ($x \geq 0.2$). From the TPD profiles, it is possible to calculate the rate and amount of O_2 desorbed for each samples from 400 to 973 K, which involves alpha and beta species. This amount has been plotted as a function of calcium substitution and the results are displayed in Fig. 6. A continuous increase in the amount of oxygen desorbed is observed as Ca^{2+} content increase in the citrate method; whereas the value maximizes at $x = 0.2$ in the basic series. For larger amounts of Ca, the amount of O_2 uptake remains virtually constant. This feature may be explained considering that a large amount of La can be substituted by Ca

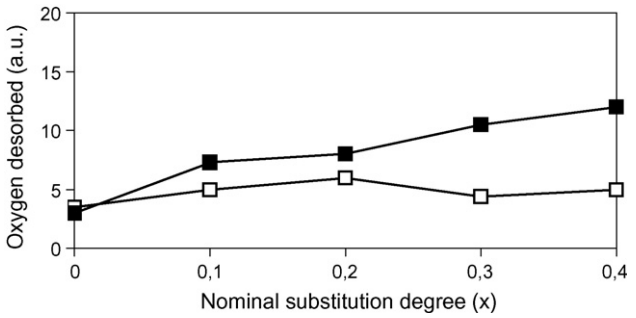

Fig. 6. Oxygen TPD desorbed/g as a function of the substitution degree: (□) basic method; (■) citrate method.

when $LaFeO_3$ perovskites are prepared using in citrate method. Therefore, a large amount of lattice oxygen in the bulk desorbed from the samples indicates a large substitution vacancy and/or defects. The trends observed in the variation with x of oxygen desorption and the similarity of TPD profiles for the citrate method is in line with previous results reported for $La_{1-x}Sr_xFeO_3$ [25] prepared by the acetate route. The results of O_2 TPD show that the amount of oxygen evolved is closely proportional to the calcium ions incorporated to the perovskite structure.

In order to add more information to the observed differences in the perovskite structure, temperature-programmed reduction and oxidation cycles were performed with the calcined samples. A first reduction step under H_2/Ar flow was carried out up to 973 K (TPR_1). Then it was cooled down in Ar flow to room temperature and an O_2/He flow it was switched to the reactor. Once the base line was restored, a programmed oxidation was carried out up to 973 K (TPO). Then, the sample was cooled down again and a second reduction treatment was performed (TPR_2). This procedure was selected to study the thermal stability of the prepared perovskites under hydrogen.

In general, the TPR_2 profile is more complex and different from TPR_1, indicating changes of the perovskite after treatment in hydrogen at 1000 K. For the basic series, the TPR_1 profiles of the pure $LaFeO_3$ perovskite and the one with $x = 0.1$ do not present any reduction peak, while a single, well-defined peak that is centred at 690 K appears when $x \geq 0.2$, increasing intensity as the calcium substitution increases. The TPR_2 profiles for the pure $LaFeO_3$ perovskite exhibit features similar to those of TPR_1, but present from 373 to 773 K a very small, broad peak without a defined maximum. This is indicative of the high stability of the non-substituted perovskite structure. Fig. 7(a) and (b) displays the TPR_1 and TPR_2 profiles of the perovskites prepared by the citrate method. $LaFeO_3$ shows almost no reduction peaks, whereas the TPR_1 for the substituted perovskites shows a large, defined peak at lower temperatures and that shifts to higher temperatures and increases in intensity as calcium substitution increases. The replacement of part of La by Ca to produce $La_{1-x}Ca_xFeO_3$ leads to a change in the nature of the phases that make up the perovskite. Initially, the citrate-prepared perovskites are pure phases with a composition close to stoichiometry. A partial reduction of Fe^{3+} to metallic iron occurs during TPR_1, resulting in a defective perovskite with vacancies. Subsequently, the metallic iron expelled from the perovskite structure during TPR_1 is re-oxidised into iron oxide during oxidation (TPO), resulting in a non-stoichiometric perovskite plus iron oxide. Consequently, TPR_2 has signals that correspond to a perovskite plus iron oxide. Two defined peaks, the larger at 520 K with a slight shift to higher temperatures as calcium substitution increases, followed by a second broad, small peak at 620 K. At higher temperatures, the hydrogen consumption increases linearly with temperature and no maximum could be detected up to 973 K. In the TPR_2 profiles of these samples, the first peak increases in intensity and the broad peak is transformed into a well-defined peak centred at 620 K before the usual increases in the hydrogen consumption with temperature up to 973 K. The differences observed in the

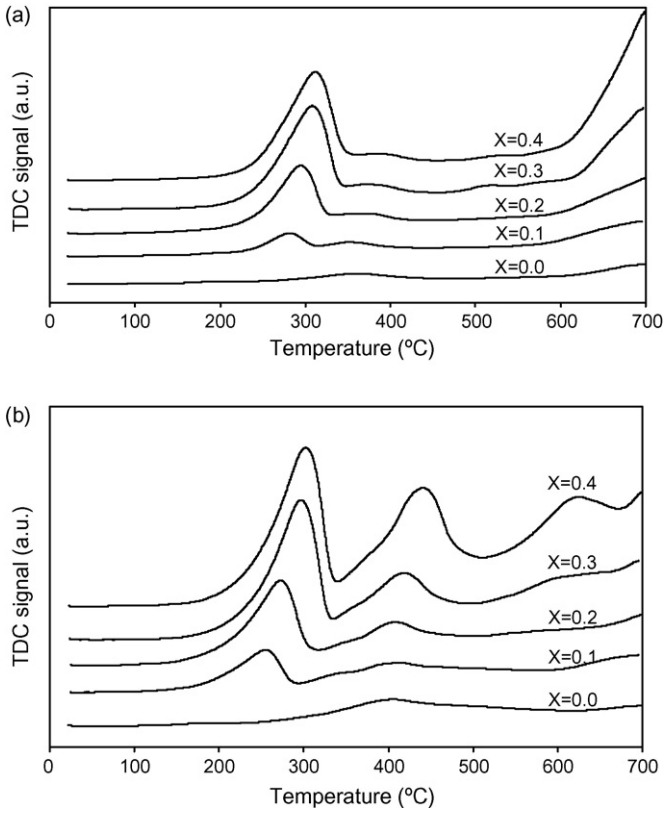

Fig. 7. Temperature-programmed reduction profiles of $La_{1-x}Ca_xFeO_3$ perovskites prepared by the citrate method: (a) TPR_1; (b) TPR_2.

TPR profiles can be interpreted as in the samples prepared by a basic method: the perovskite structure only allows a small amount of substitution of Ca by La ($x = 0.1$), and calcium is present as a segregated phase for larger values of x. Thus, the hydrogen consumption in the TPR_1 is required to reduce the bulk of segregated Fe_2O_3 present due to the small amount of Ca substituted by La. A different situation occurs in the samples prepared via citrate. The higher hydrogen consumption when the calcium substitution increases can be explained by the higher Fe^{4+} ions amount generated to compensate the charge unbalance [16,17]. This is in line with the XRD results. Fig. 8 displays the H_2 consumption up to the end of the second peak as a function of the substitution degree for both perovskite series.

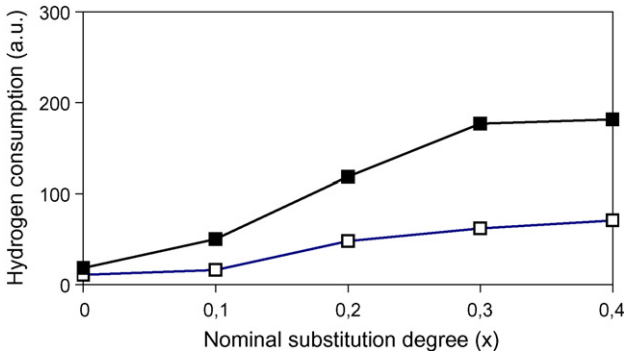

Fig. 8. Hydrogen consumption as a function of the substitution degree: (□) basic method; (■) citrate method.

For the samples prepared by the basic method, the H_2 uptake is lower with a slight increase when x varies from 0.1 to 0.2. Much higher hydrogen consumption can be observed for the citrate series, possibly accounting for the higher surface area of this series. Additionally, when compared to the basic series, the trend is slightly different, indicating that the substitution of calcium in the $LaFeO_3$ lattice is different and leads to a greater insertion of Ca^{2+} ions, as was previously discussed. To detect possible modification in the perovskite structure during TPR experiments as a consequence of the reduction, once the TPR_1 was finished, the reducing gaseous mixture was shifted by helium flow and cooled down to room temperature. The sample was kept in an inert atmosphere and transferred to the XRD camera. Fig. 9(a) and (b) shows two representative diffractograms obtained in these circumstances for the simple $LaFeO_3$ perovskite and a representative $La_{1-x}Ca_xFeO_3$ perovskite prepared via the citrate method. It can be observed that the XRDs are practically equal for both fresh and after TPR_1, suggesting that the structure does not change after hydrogen treatment although the nature of the phases composing the sample changes. The simple perovskites (Fig. 9(a)) present essentially the same diffraction lines found for the fresh perovskite with only an increase in the intensity of the peaks and small shifts towards lower angles, indicating increased crystallinity with a great expansion of the cell parameters. The specific area of the perovskites shows a decrease lower than 10% as expected for more crystalline solids. The substituted perovskites (Fig. 9(b)) present virtually the same behaviour with the presence of a new peak at $2\theta = 45^\circ$ corresponding to Fe°. It has been pointed out that BET surface area data show that these materials suffer from sintering during successive cycles decreasing their surface areas lower than 1 $m^2\,g^{-1}$ [26]. The results of the TPR_1, TPO and TPR_2 cycles allow the

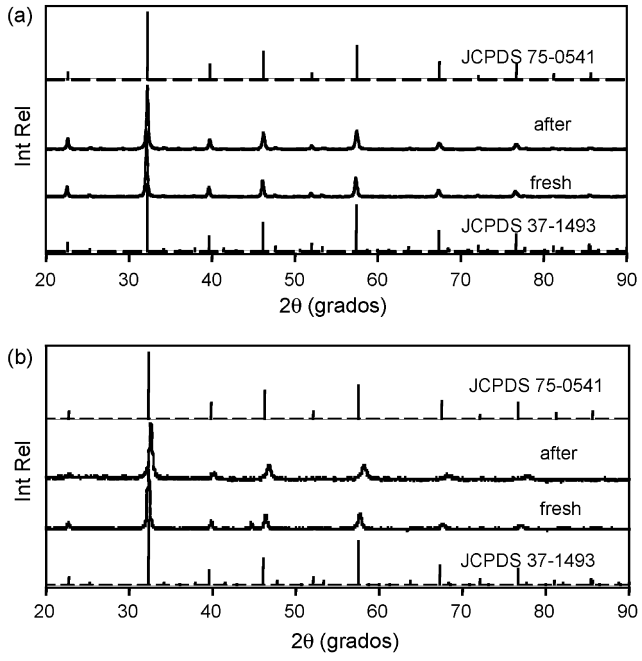

Fig. 9. XRD patterns fresh and after TPR_1 of $La_{1-x}Ca_xFeO_3$, perovskites: (a) $x = 0.0$, (b) $x = 0.4$.

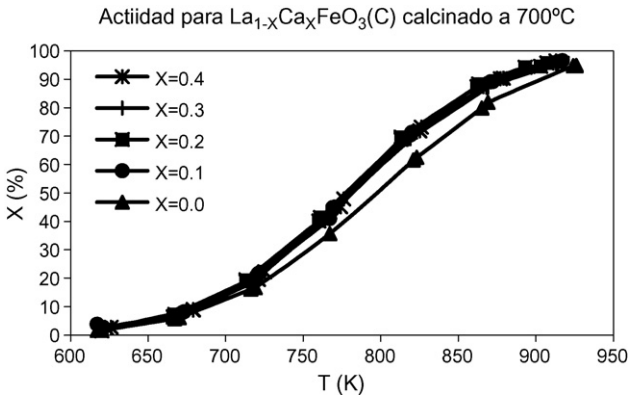

Fig. 10. Stationary-state conversion over $La_{1-x}Ca_xFeO_3$ perovskites.

conclusion that the substitution of $LaFeO_3$ perovskites with calcium weakens the structure, and that this destruction is irreversible under reductive conditions.

3.1. Catalytic activity

The prepared perovskites were evaluated in methane and acetyl acetate oxidation in a flow reactor using an excess of oxygen. Carbon dioxide and water were the only observed products for the methane combustion and smaller traces of acetaldehyde were also obtained in the acetyl acetate combustion, without dependence on the calcium substitution. No CO was detected for the studied perovskites. Fig. 10 shows the dependence of methane and acetyl acetate conversion on the reaction temperature for the different perovskites. The ignition temperature (T_{50}), defined as the temperature required to obtain 50% conversion, and the intrinsic activity expressed as mole converted per second and gram of catalyst evaluated at 593 K for acetyl acetate and 723 K for methane are given in Table 2. These data show different trends in the change of the activity of the prepared perovskites as a function of Ca substitution. For the basic series, a decrease in the ignition temperature without changes in the degree of substitution was observed for the methane reaction, while an increase can be observed for the acetyl acetate reaction. Different behaviour was observed for the citrate-prepared perovskites, detecting almost no change in the ignition temperature with calcium substitution for the methane reaction and a decrease for the acetyl acetate reaction.

Table 2
Ignition temperature (T_{50}) and intrinsic activity in acetyl acetate and methane combustion for $La_{1-x}Ca_xFeO_3$ perovskites

	T_{50} (K)		Intrinsic activity (mol g^{-1} s^{-1} × 10^5)	
	Acetyl acetate	Methane	Acetyl acetate, 593 K	Methane, 723 K
$LaFeO_3$-B	588	881	12.5	1.1
$La_{0.9}Ca_{0.1}FeO_3$-B	625	790	3.1	3.0
$La_{0.8}Ca_{0.2}FeO_3$-B	629	803	1.4	2.9
$La_{0.7}Ca_{0.3}FeO_3$-B	641	781	2.1	2.7
$La_{0.6}Ca_{0.4}FeO_3$-B	633	783	2.1	2.7
$LaFeO_3$-C	613	781	6.2	3.5
$La_{0.9}Ca_{0.1}FeO_3$-C	598	778	9.2	3.9
$La_{0.8}Ca_{0.2}FeO_3$-C	593	776	10.3	4.1
$La_{0.7}Ca_{0.3}FeO_3$-C	589	778	11.3	4.1
$La_{0.6}Ca_{0.4}FeO_3$-C	587	783	11.9	3.3

To clarify these trends, the intrinsic activity of the prepared perovskites as a function of calcium substitution is shown in Table 2. The intrinsic activity in the methane combustion is almost the same value for all the substituted perovskites, without a preparation method effect. Thus, in this reaction, the extent of the reaction seems to be independent of the characteristic of the active site in line with results previously reported for Sr-substituted lanthanum manganites [27] for the methane combustion. The beta oxygen appears in the O_2 DTP at higher temperatures and up to 700 K. Therefore, the evolution has not been completed, and it is not possible to quantify the amount of these types of oxygen site. Consequently, conclusions on the dependence on the activity in these given reactions with this type of oxygen are difficult. For the acetyl acetate reaction, a decrease in the reaction rate for the basic series and an increase for the citrate method can be observed. Thus, the opposite trends displayed by these perovskite series can be explained on the basis of their characterization results. Therefore, it can be concluded that the presence of substituted calcium ions in the perovskite structure improves the catalytic activity in the acetyl acetate combustion and modified slightly the activity in the methane combustion. These behaviours support the idea that each reaction probably occurs through a different reaction mechanism.

4. Conclusions

The results obtained in the present research show that a continuous substitution of calcium by lanthanum in a $La_{1-x}Ca_xFeO_3$ ($x = 0.0$, 0.1, 0.2, 0.3, 0.4) perovskite-type oxide structure is reached via the citrate method, while the substitution can occur only for $x < 0.2$ and traces of a segregated phase of $CaCO_3$ for $x \geq 0.2$ via the basic method. Under the used experimental conditions, the substituted perovskites exhibited lower activity than the simple $LaFeO_3$ perovskite in the methane combustion, without effect of the preparation method or the extent of substitution.

For the acetyl acetate combustion, the activity depends on the degree of substitution, where the most active citrate perovskite is the one with the highest substitution degree. For the basic method, the activity decreases as the substitution degree increases up to $x = 0.2$, reaching activity independent on the x value. These results are in line with those provided by the characterization results that indicate the low substitution degree exhibited by the samples obtained by the basic medium. Therefore, it should be pointed out that the insertion of calcium ions into the perovskite lattice leads to a solid with structural and electronic defects and which provide sites with higher activity in redox reactions. This result can be clearly seen in acetyl acetate combustion, which occurs at a lower temperature, but not in the methane combustion which requires a much higher temperature and takes place under a different reaction mechanism. The perovskite activity depends on the composition, the preparation method, and the nature of the substrate used in the combustion.

Acknowledgements

The authors thank CONICYT (Fondecyt Grant 1060702) from Chile and CONICET, ANPCyT and the Universidad Nacional de San Luis from Argentina for financial support.

References

[1] W.F. Libby, Science 171 (1971) 499.
[2] M. ÓConnell, A.K. Norman, C.F. Hüttermann, M.A. Morris, Catal. Today 47 (1999) 123.
[3] L.J. Tejuca, J.L.G. Fierro, in: Marcel Dekker (Ed.), Properties and Applications of Perovskite-Type Oxides, New York, 1993.
[4] R.J.H. Voorhoeve, in: H.H. Burton, R.L. Garten (Eds.), Advanced Materials in Catalysis, Academic Press, New York, 1977, , p.127.
[5] S. Irusta, M.P. Pina, M. Melendez, J. Santamaría, Catal. Lett. 54 (1998) 69.
[6] L.G. Tejuca, J.L.G. Fierro, J.M.D. Tascón, Adv. Catal. 36 (1989) 237.
[7] Y. Wu, T. Yu, B.S. Dou, C.X. Wang, X.F. Xie, Z.L. Yu, S.R. Fan, Z.R. Fan, L.C. Wang, J. Catal. 120 (1989) 88.
[8] V.V. Kharton, A.A. Viskupa, E.N. Naumovicha, V.N. Tikhonovicha, Mater. Res. Bull. 34 (1999) 1311.
[9] Z. Yu, L. Gao, S. Yuan, Y. Wu, J. Chem. Soc. Faraday Trans. 88 (1992) 3245.
[10] C.N.R. Rao, J. Gopalakrishnan, New Directions in Solid State Chemistry, Cambridge University Press, Cambridge, 1997, p. 53.
[11] N. Yamazoe, Y. Teraoka, Catal. Today 8 (1990) 176.
[12] R. Sumathi, K. Johnson, B. Viswanathan, T.K. Varadarajan, Appl. Catal. A 172 (1998) 15.
[13] H. Taguchi, J. Solid State Chem. 124 (1996) 360.
[14] M. Popa, J. Frantti, M. Kakihana, Solid State Ionics 154 (2002) 437.
[15] P. Ciambelli, S. Cimino, L. Lisi, M. Faticanti, G. Minelli, I. Pettiti, P. Porta, Appl. Catal. B 33 (2001) 193.
[16] P. Ciambelli, S. Cimino, S. De Rossi, M. Faticanti, L. Lisi, G. Minelli, I. Pettiti, P. Porta, G. Russo, M. Turco, Appl. Catal. B 24 (2000) 243.
[17] B.P. Barbero, J. Andrade Gamboa, L.E. Cadús, Appl. Catal. B 65 (2006) 21.
[18] R.D. Shannon, Acta Cryst. A 32 (1976) 751.
[19] H. Chang, Chin. J. Phys. 34 (1996) 310.
[20] A. Davydov, Infrared Spectroscopy of Adsorbed Species on the Surface of Transition Metal Oxides, Wiley, England, 1990 (Chapter 1).
[21] D. Berger, V. Fruth, I. Jitaru, J. Schoonman, Mater. Lett. 58 (2004) 2418.
[22] M. Imamura, N. Matsubayashi, H. Shimada, J. Phys. Chem. B 104 (2000) 7348.
[23] N.A. Merino, B.P. Barbero, P. Grange, L.E. Cadús, J. Catal. 231 (2005) 232.
[24] Z. Zhao, X. Yang, Y. Wu, Appl. Catal. B 8 (1996) 281.
[25] T. Nitadori, M. Misono, J. Catal. 93 (1985) 459.
[26] S. Irusta, M.P. Pina, M. Melendez, J. Santamaría, J. Catal. 179 (1998) 400.
[27] S. Ponce, M.A. Peña, J.L.G. Fierro, Appl. Catal. B 24 (2000) 193.